A Damage Localization Method With Multimodal Lamb Wave Based on Adaptive Polynomial Chirplet Transform

Zhe Wang, Songling Huang, *Senior Member, IEEE,* Shen Wang, Qing Wang, *Senior Member, IEEE,* and Wei Zhao

Abstract—**Ultrasonic Lamb wave testing allows health monitoring for plate structures and has been extensively applied in the modern industry. To obtain the location and further form the damage imaging, the time of flight (TOF) is a pivotal parameter. However, the dispersive and multimodal nature of the Lamb wave obstructs the accurate measurement of TOF. The objective of this article is to develop efficient techniques to separate multimodal Lamb wave signals and accomplish accurate damage localization. The narrowband Lamb wave is generated by the excitation signal with a center frequency of 150 kHz. The fundamental symmetric and antisymmetric modes are exploited. The adaptive polynomial chirplet transform (CT) is proposed to decompose the Lamb wave signals and identify the modes. Then, the instantaneous frequency characteristics are utilized to extract time information. Thus, the TOF is obtained and damage location can be calculated. The reconstruction error is defined to quantitate the difference between the reconstructed signal and the received signal. The obtained reconstruction errors from the simulation and experiment are 0.1631 and 0.2875, respectively. The varied defect location is adopted to obtain the TOF estimation. The results show that the proposed method outperforms the CT and cross correlation, especially for the longer propagation distances where the dispersion effect is distinct. For experiments considering the defect and boundary reflection, the localization errors of the collinear defect are 2.51% and 3.04% for the two Lamb wave modes. In comparison with smoothed-pseudo-Wigner–Ville distribution and CT, the proposed method owns superior performance on mode identification and location accuracy.**

***Index Terms*—Damage localization, Lamb wave, mode separation, time of flight (TOF).**

I. INTRODUCTION

THE structure damage occurs in the modern industry and threatens the normal operation of instruments. For example, the corrosion and erosion will lead to the thinning Effects on the aluminum aircraft structural stringers and storage tanks [1], [2]. Ultrasonic guided wave testing provides an effective approach to inspecting the health status of structure [3] – [6]. Guided wave is a mechanical wave that can propagate along the specific structure for a long distance with little energy loss. Lamb wave is one kind of guided wave and it exists in a plate. The vibration of the Lamb wave covers the whole plate thickness [7]. It can be utilized to detect both the internal and the surface damage [8]. These advantages make Lamb wave a preferable method in plate inspection.

Lamb wave can be generated by electromagnetic acoustic transducers (EMATs) or piezoelectric transducers. When the Lamb wave encounters the discontinuities in its propagation path, the reflection and transmission will occur. Thus, the received Lamb wave contains useful information about the health status in its route. Through extracting the features of received Lamb wave, the metallic welds could be detected and the quality can be evaluated using a neural classifier [9]. Among the features, time of flight (TOF) is the commonly used information to determine the location [10]–[12]. The Wigner–Ville distribution (WVD) was applied to calculate the TOF of Lamb wave to accomplish the damage localization [13]. The wavelet transform was adopted to extract the time information in noisy environments [14]. The wavelet network was designed to utilize the TOF, amplitude, and wave area of Lamb wave to estimate the location and severity of damage [15]. However, these methods had not considered the identification of multimodal Lamb wave.

The multimodal and dispersive characteristics of Lamb wave deteriorate the accurate measurements of TOF [16], [17]. The effect of dispersion had been investigated and dispersion compensation algorithm had already been designed [18]–[20]. Mode selection is conducted by considering the basic factors, such as attenuation and sensitivity [21]. The comb transducer and interdigital transducer had been designed to produce specific modes by controlling the spacing in the transduction element [22], [23]. The interval in the meander coil of EMAT is designed to control the generated mode [24]. Several methods had also been developed to process the multimodal Lamb wave signals. The chirplet matching pursuit (MP) was conducted to decompose the multimodal Lamb wave in the chirplet atoms [25]. However, the linear time–frequency behavior of atoms did not represent Lamb wave well. The cross-WVD of the excitation signal and received signal was employed to separate the mode components and reflected components, but it did not distinguish the modes [26]. The ridge tracking and Vold–Kalman filter were applied to isolate interfered wave modes

Z. Wang, S. Huang, S. Wang, and W. Zhao are with the State Key Laboratory of Power System, Department of Electrical Engineering, Tsinghua University, Beijing 100084, China (e-mail: huangsling@mail.tsinghua.edu.cn).

Q. Wang is with the Department of Engineering, Durham University, Durham DH1 3LE, U.K.

generated from broadband excitation signal [27], [28]. However, the broadband Lamb wave caused more modes and complicated overlapping. The empirical mode decomposition (EMD) and short-time Fourier transform were combined to recognize the overlapped signal, but the process of EMD did not separate the direct wave and reflected signal of the same mode [29]. Therefore, further research needs to be conducted to analyze multimodal Lamb wave signals.

In this article, the accurate damage localization method is proposed based on the separation of multimodal Lamb wave signals with narrow band. The aim is to characterize the dispersive nature and represent the Lamb wave signal despite the different propagation distances. The adaptive polynomial chirplet transform (ACPT) is designed to analyze the dispersive Lamb wave signal. The multimodes can be decomposed into individual modes by the polynomial chirplet basis functions. Then, the time information corresponding to the excitation frequency can be extracted from the instantaneous frequency (IF) of individual modes. Then, the accurate TOF can be obtained and the damage location can be calculated. Both the simulations and experiments are conducted to verify the effectiveness of the proposed method.

The remainder of this article is organized as follows. Section II analyzes the multimodal and dispersive characteristics of Lamb wave. In Section III, the mode decomposition algorithm is proposed and its procedures are summarized in detail. In Section IV, the principle of damage localization is presented. Then, the performance of the proposed method is evaluated by simulation analysis and experimental investigations in Section V. The performance of the proposed ACPT is also compared with those from commonly used chirplet transform (CT), cross correlation (CC), and smoothedpseudo-WVD. Concluding remarks are given in Section VI.

II. MULTIMODAL AND DISPERSIVE CHARACTERISTICS OF LAMB WAVE

Compared with an ultrasonic bulk wave, Lamb wave owns more complicated characteristics. Bulk wave is divided into transverse and longitudinal waves. Its velocity is influenced by material property. However, the generated Lamb wave modes and their velocities are influenced by the excitation frequency and plate thickness.

A. Multimodes Coexisting

According to the different displacement components, Lamb wave is decoupled into two types: symmetric mode (*S* mode) and antisymmetric mode (*A* mode). These two types can be expressed by the Rayleigh–Lamb equation [7]. The equation can only be solved by a numerical method. The solutions are infinite and the results can be denoted as

$$S \text{ mode}: \ S_n, \quad n = 0, 1, 2, \ldots \tag{1}$$

$$A \text{ mode}: \ A_n, \quad n = 0, 1, 2, \ldots. \tag{2}$$

The displacement of Lamb wave can be depicted by wave structure. The wave structures of different modes vary with the wave frequency and plate thickness. For the steel plate with Young's modulus of 205 GPa and Poisson's ratio of 0.3 and density of 7850 kg.m-3, the wave structures of S_0 and A_0 mode are shown in Fig 1, where *d* is the plate thickness, *u* is the in-plate displacement, and *v* is the out-of-plane displacement.

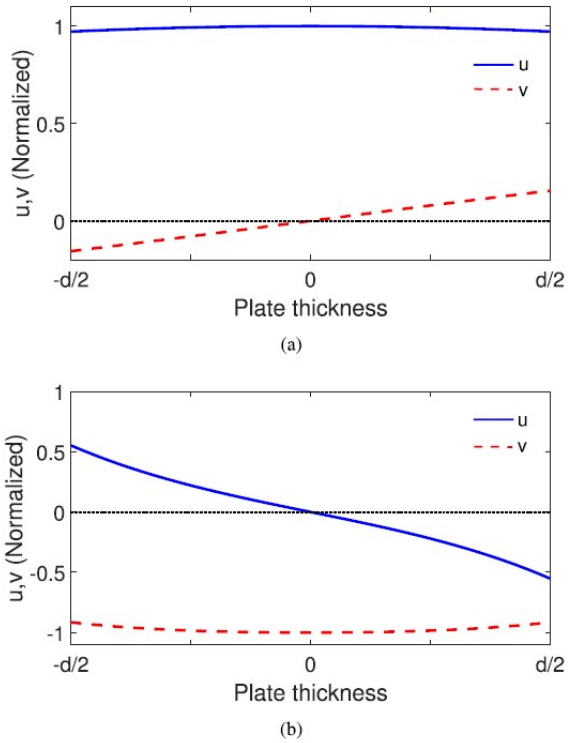

Fig.1. Displacement symmetry of S mode is opposite to that of A mode. (a) Wave structure for S_0 mode. (b) Wave structure for A_0 mode.

Apart from the coexisting of *S* and *A* modes, mode conversion occurs when Lamb wave encounters damage in plate. For example, after the interaction of *S* mode and the irregular defect, *A* mode will be generated by the mode conversion. In the reflected wave, both *S* and *A* modes can be detected [30], [31]. Therefore, multimodes might bring severe interference when applying the Lamb wave.

B. Dispersion Phenomenon

The phase velocity of Lamb wave is defined as $c_p = \omega/k$. The group velocity c_g can be derived from phase velocity and expressed as $c_g = d\omega/dk$. According to the Rayleigh–Lamb equation, the phase velocity and the group velocity can be presented as the function of product of frequency and plate thickness. Fig. 2 shows the numerical results. As the increase of the product of frequency and plate thickness, more modes exist in plate. The lowest frequency for the higher mode is known as the cutoff frequency. With the plate thickness of 4 mm, the frequency of 150 kHz is chosen to avoid the interference of higher modes. Thus, only S_0 and A_0 modes are considered in the following research. According to the frequency and phase velocities, the wavelengths for these two modes are 35.6 and 13.3 mm, respectively.

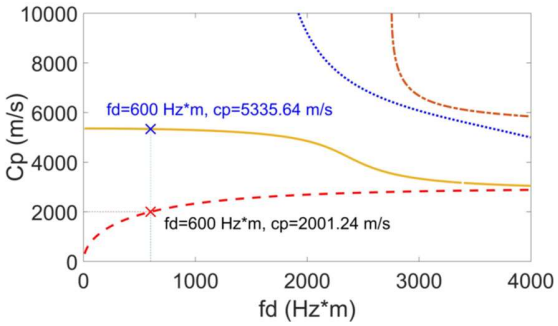

(a)

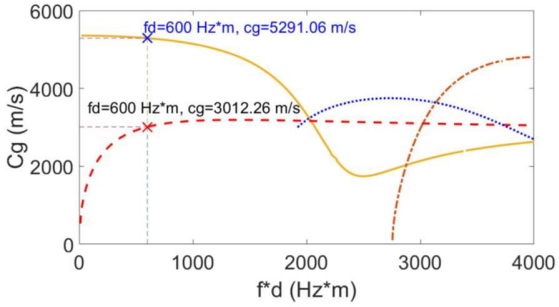

(b)

Fig.2. Dispersion curve for Lamb wave. The phase velocity and group velocity vary as a function of the product of frequency and plate thickness. (a) Phase velocity. (b) Group velocity.

Since the velocity varies with thickness, the time information can be utilized to analyze the wall thinning in structure. This is the advantage of dispersion which can help to diagnose the plate structure. However, for the frequency of excitation signal owns a bandwidth, the dispersion will lead to the dilation of wavepackets in time domain. Thus, the wavepackets of the direct wave and the reflection wave from discontinuous sections are easily overlapped. This brings the challenge to interpret the received signal.

III. MODE DECOMPOSITION ALGORITHM

The block diagram for the mode decomposition and damage localization method is summarized in Fig. 3. The multimodal Lamb waves require to be separated into individual modes first. In Sections III-A–III-C, the details of the proposed decomposition algorithm will be described.

A. Excitation Signal

To generate the Lamb wave, the excitation signal is loaded on the transducer. The windowed tone burst is chosen as the excitation signal, which has the form of

$$x(t) = w(t)\sin(2\pi f_c t) \tag{3}$$

where $\omega(t)$ is the window function and f_c is the center frequency. The excitation signal usually has a short time duration and the truncation effect leads to spectrum leakage.

TABLE I
OPERATIONS TO THE UNITARY GAUSSIAN FUNCTION

Four Different Operations	Corresponding Parameter	Expression
Scaling	s	$\frac{1}{\sqrt{s}} g(\frac{t}{s})$
Time Shift	t_0	$g(t-t_o)$
Frequency Shift	ω_0	$e^{jw_0 t}$
Chirping	5	$g(t)e^{jct^2}$

The added window function can help to decrease the leakage. In this article, the Hanning window is adopted and its expression is

$$w(t) = \left(H(t) - H\left(t - \frac{N}{f_c}\right)\right)\left(0.5 - 0.5\cos\frac{2\pi f_c t}{N}\right) \tag{4}$$

where $H(t)$ is the step function and N is the cycle number of the window. For the six-cycle Hanning windowed tone burst with a center frequency of 150 kHz, Fig. 4 shows the signal and corresponding spectrum. It is clear that the excitation signal has a limited bandwidth and the highest amplitude lies in the center frequency.

B. Adaptive Polynomial Chirplet Transform

After the excitation of Lamb wave, *S* and *A* modes coexist in the plate structure. The received signal may be overlapped in time domain and thus makes the modes hard to be separated. However, different modes have distinguished characteristics in the time–frequency domain. The polynomial Gaussian chirplet owns "customized" time–frequency characteristics to represent the Lamb wave signal. For the defect localization, it is enough to extract the corresponding TOF from the time–frequency domain. Therefore, the polynomial Gaussian chirplet contains abundant information to analyze the Lamb wave signal and it is considered as the basis function in the proposed ACPT.

The conventional CT utilizes the Gaussian windowed chirp signal. The unitary Gaussian function is given in (5). The chirplets are derived by employing different operations to the unitary function

$$g(t) = \frac{1}{\pi^{\frac{1}{4}}} e^{-\frac{t^2}{2}}. \tag{5}$$

The four operations are summarized in Table I. Compared with the short-time Fourier transform and wavelet transform, the conventional CT increases the "chirping" operation to the basis function, and thus, it can describe the signal more accurately. Combined the four operations by setting adjustable parameters, the Gaussian chirplet is expressed as

$$g_{s,t_0,\omega_0,c} = \frac{1}{(\pi s^2)^{\frac{1}{4}}} e^{-\frac{(t-t_0)^2}{2s^2}} \cdot e^{j\omega_0(t-t_0)} \cdot e^{jc(t-t_0)^2}. \tag{6}$$

The effects of the operations are shown in Fig. 5. The results are shown in the time–frequency domain. As the figures show, the operations not only adjust the location of Gaussian basis function in the time-frequency domain but also the changing rate of frequency.

The CT provides a solution to represent signals with linear

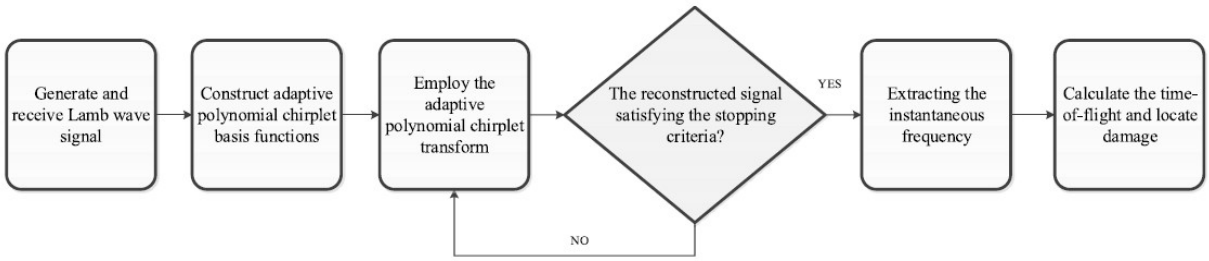

Fig. 3. Block diagram of the proposed method. The multimodal Lamb wave signals are first separated into individual modes, and then, the TOF is extracted from the IF. The damage location is calculated from the TOF and velocity.

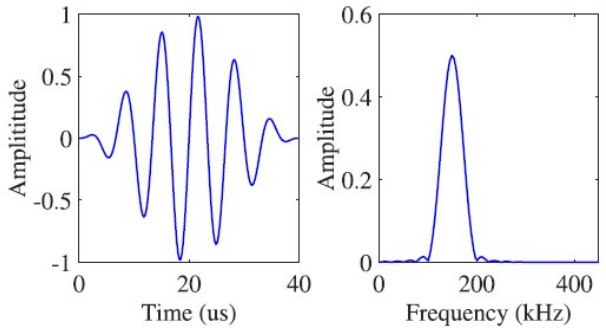

Fig.4. Six-cycle excitation signal and the corresponding spectrum. The signal has a limited bandwidth.

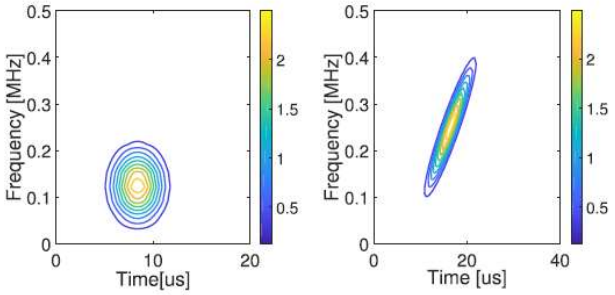

Fig. 5. Time-frequency representation of the effect of the operations. Left: unitary Gaussian chirplet. Right: employing the scaling, time shift, frequency shift, and chirping on the unitary Gaussian chirplet.

IF characteristics. However, the wave velocity of the Lamb wave signal is nonlinear with its frequency according to the dispersion relation. Lamb wave signal owns nonlinear IF characteristics and the frequency changes with different propagation distances. Thus, in the time–frequency domain, the CT is hard to track Lamb wave signal. To improve the representation capability, an adaptive polynomial Gaussian chirplet is proposed in this article. Its expression is defined as follows:

$$g_{s,t_0,\omega_0,c_k} = \frac{1}{(\pi s^2)^{\frac{1}{4}}} e^{-\frac{(t-t_0)^2}{2s^2}} \cdot e^{j\omega_0(t-t_0)} \cdot e^{j\sum_{k=2}^{n} c_k (t-t_0)^k} \quad (7)$$

where c_k is the coefficient of polynomial. The "chirping" operation changes to the form of polynomial. The purpose of polynomial is to better represent the IF of Lamb wave signal. The polynomial brings nonlinear frequency rotating operator and fits the local signal accurately. Thus, the dispersive Lamb wave signal can be decomposed into different Gaussian basis functions. The time–frequency representation for an adaptive polynomial Gaussian chirplet is shown in Fig. 6.

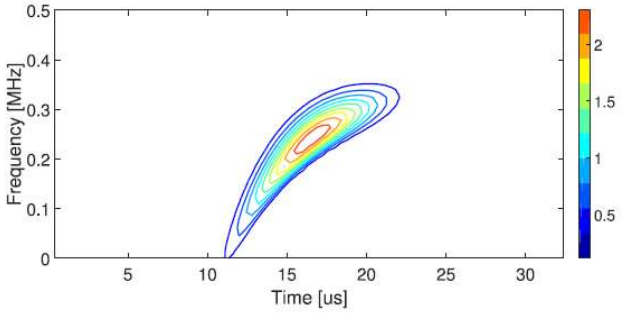

Fig.6. Time-frequency representation of an adaptive polynomial Gaussian chirplet. The frequency forms a non-linear relation with time.

Then, the APCT is defined as the inner product between the Lamb wave signal $f(t)$ and the adaptive polynomial chirplet g_{I_n} as follows:

$$\alpha_n = \langle f, g_{I_n} \rangle = \int_{-\infty}^{+\infty} f(t) g_{I_n}^*(t) dt \quad (8)$$

where "*" denotes the conjugate operation and α is onsidered as the projection of signal on specific chirplet basis function g_{I_n}. The index set $I_n = [s, t_0, \omega_0, c_k]$ is the combination of parameters. Therefore, Lamb wave signal is constructed as a weighted combination of adaptive polynomial chirplet basis functions, which can be expressed as follows:

$$f(t) = \sum_{n=1}^{P} \alpha_n g_{I_n} + r_p \quad (9)$$

where P is the number of decomposed basis function and r_p is the residue after iterations.

If the signal of multiple modes overlapped in time domain, two or more adaptive polynomial chirplet basis functions will

be found to make up the signal. If the wavepacket only contains one Lamb wave mode, then the value of P will be equal to one and only one basis function matches the signal most.

C. Mode Identification

To decompose the overlapped signal and obtain the corresponding modes, the dictionary containing basis functions is very significant to describe the Lamb wave signal.

The construction of dictionary is based on the excitation signal and dispersion curve. The basis functions in the ACPT are to simulate the actual time–frequency property of Lamb wave. After solving the Rayleigh–Lamb equation numerically, the discrete sample point of the dispersion curve is obtained. For clarity of expression, the group velocity of S and A modes is marked as c_{gs} and c_{ga}, respectively. The points in the dispersion curve are notated as (f_i, c_{gsi}) and (f_i, c_{gai}) for S and A modes, respectively.

After propagating a certain distance, Lamb waves of different frequencies lie in different time domains because of their varied velocities. The time–frequency characteristic of Lamb wave signal is represented as (f_i, t_{si}) and (f_i, t_{ai}) for S and A modes, respectively. To fit the relation of discrete-time sample point and discrete frequency point using a least-square approach, the coefficient c_k in the polynomial can be obtained. It is worth noting that the discrete frequency point is chosen to cover the frequency of the Lamb wave signal. The center frequency of excitation signal lies in the middle value of the chosen frequency point. Thus, the derived basis function can represent the generated Lamb wave. By repeating this process, the corresponding coefficient c_k will be constructed and the adaptive polynomial basis function will be achieved. Besides, the time- and frequency-shifting operations are imposed on the basis function to change its time–frequency center. The scaling operation is also employed to change the spread of basis function.

Once the dictionary is obtained, the optimal g_{I_n} and α can be solved according to the predefined basis functions. It is the famous NP-hard problem to solve (8). For the specific Lamb wave signal, g_{I_n} is predefined by the set I_n and thus decreases the search space. The MP technique is applied to decompose the Lamb wave signal into designed basis functions.

In the process of MP, the signal of wavepacket is projected on each basis function in the dictionary. The amplitude of α_n is used to decide the optimal basis functions. After the first iteration, the largest α_n and corresponding g_{I_n} will be chosen as the decomposed component from the signal. Then, the extracted component will be subtracted from the original signal to obtain the residual. The residual is considered as the signal and continues to repeat the MP technique. The iteration is finished until the residual achieved the stopping criteria

$$f(t) - \sum_{n=1}^{P} \alpha_n g_{I_n} < \epsilon \tag{10}$$

Where ϵ is the designed error of reconstruction. Since the basis function in the dictionary represents S mode or A mode after propagating certain distance, the overlapped signal will be successfully decomposed into individual modes. By comparing the index set of I_n with that in the dictionary, the mode can be determined.

IV. PRINCIPLE OF DAMAGE LOCALIZATION

A. Instantaneous Frequency

IF provides an effective tool to describe the nonstationary Lamb wave signal. To understand IF, the concept of the analytic signal is given first.

The analytic signal is complex-valued. For real-valued signal $x(t)$, it can be converted into its corresponding analytic form by the Hilbert transform. The Hilbert transform of $x(t)$ is

$$\hat{x} = x(t) * \frac{1}{\pi t} = \frac{1}{\pi} \int_{-\infty}^{+\infty} \frac{x(\tau)}{t-\tau} d\tau. \tag{11}$$

Then, the analytic signal is

$$z(t) = x(t) + j\hat{x}(t) = a(t)e^{j\varphi(t)} \tag{12}$$

where $a(t)$ is known as the instantaneous amplitude and $e^{j\varphi(t)}$ is known as the instantaneous phase. For complex-valued signal $x(t)$, it can also be denoted as the form of $a(t)e^{j\varphi(t)}$.

Similar to the frequency of stationary signal, the IF of a signal $x(t)$ is given as the derivative of the phase of corresponding analytic signal $z(t)$ [32]

$$f_i(t) = \frac{1}{2\pi}\frac{d}{dt}\arg(z(t)) = \frac{1}{2\pi}\frac{d\varphi(t)}{dt}. \tag{13}$$

Through the Hilbert transform to present the signal phase explicitly, the IF of both complex- and real-valued signals can be obtained using (13).

For the basis functions in the chirplet dictionary, it has the form of complex value and the phase is defined as follows:

$$\phi(t) = \omega(t - t_0) + \sum_{k=2}^{n} c_k (t - t_0)^k. \tag{14}$$

Then, the IF of basis function can be expressed as

$$\mathrm{IF}(t) = \frac{1}{2\pi}\frac{d\phi(t)}{dt} = \frac{1}{2\pi}\left[\omega + \sum_{k=2}^{n} k c_k (t - t_0)^{k-1}\right]. \tag{15}$$

After the signal is separated by the MP technique, each mode of Lamb wave signal is represented by the basis function. Then, the time–frequency characteristic of individual mode is also obtained. Through extracting the time information corresponding to the center frequency, the propagation time of wave and further the localization can be achieved.

B. TOF Extraction and Damage Localization

The scheme to locate the damage can be shown in Fig. 7. The transmitter to actuate Lamb wave and the receiver to sense the Lamb wave signal are placed on a steel plate. If damage exists in the propagation path, the Lamb wave will be reflected back. The receiver can not only sense the reflection echo from damage but also receive the direct wave and reflection from the boundary.

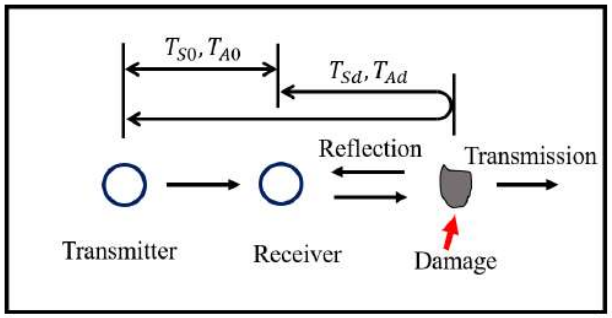

Fig. 7. Illustration of damage localization method. The distance is calculated by the product of TOF and group velocity.

After obtaining time information corresponding to the center frequency from the IF curve, the propagation time of Lamb wave can be obtained. The propagation time of direct waves is denoted as T_{S0} and T_{A0} for S and A modes, respectively. Similarly, the propagation time of reflected waves from damage are denoted as T_{Sd} and T_{Ad}, respectively. Then, the TOF from the receiver to the damage is calculated as

$$S \text{ mode}: \ \mathrm{TOF}_S = T_{Sd} - T_{S0} \tag{16}$$

$$A \text{ mode}: \ \mathrm{TOF}_A = T_{Ad} - T_{A0}. \tag{17}$$

Then, the distance between the receiver and the damage is expressed as follows:

$$S \text{ mode}: \ d = \mathrm{TOF}_S \cdot c_{sg} \tag{18}$$

$$A \text{ mode}: \ d = \mathrm{TOF}_A \cdot c_{ag} \tag{19}$$

where c_{sg} and c_{ag} are the group velocities corresponding to the center frequency. With the separation of S and A modes, both of them can be used to calculate the damage location.

V. PERFORMANCE EVALUATION OF THE PROPOSED METHOD

To verify the effectiveness of the mode decomposition algorithm and damage localization method, the corresponding simulations and experiments have been conducted. Besides, the proposed method is compared with the smoothed-pseudo-WVD and CT to prove its superiority.

A. Simulation

The finite-element analysis software of COMSOL Multiphysics is adopted to simulate the propagation of Lamb wave in plate. The 3-D plate model is constructed in the software. The material parameters of plate are from the steel which already used in the before-mentioned dispersive characteristic analysis. The plate thickness is set as 4 mm.

1) Case I: The Overlapping by Boundary Reflection: The Hanning windowed tone burst is loaded on the excitation point that is in the center of plate. The center frequency and cycle number of the tone burst are 150 kHz and 6, respectively. From the spectrum in Fig. 4, it can be observed that the frequency components are concentrated in the main lobe and this lobe owns the highest amplitude. Although the sidelobes exist, their amplitudes are rather small and the largest frequency of the first sidelobe is still lower than 230 kHz. According to the dispersion curves, the excitation frequency is less than the cutoff frequency of higher modes. Thus, the fundamental S and A modes will be generated according to the Rayleigh–Lamb equation.

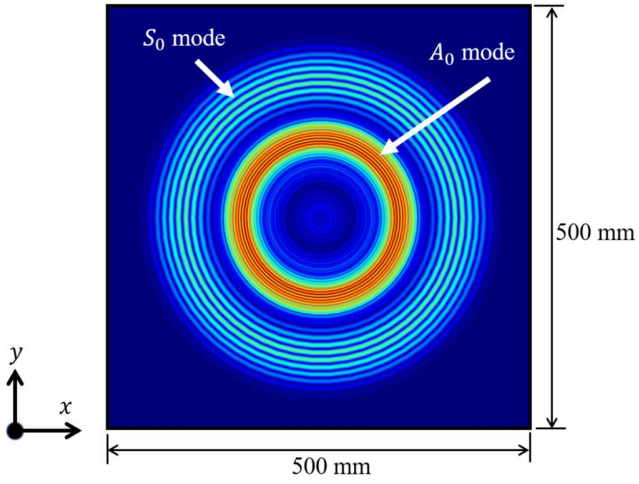

Fig.8. Total displacement captured at 84 μs in the simulation. Two modes coexist with different propagation velocities.

The receiver point is set 400 mm away from the excitation point. The boundaries of plate except the right boundary are set as low-reflecting boundaries to reduce the wave intervention. The right boundary is in the right of the receiver with a distance of 200 mm, and the reflection wave from the right boundary is studied in this case. Fig. 8 shows the total displacement of the Lamb wave, which is captured at 84 μs in the simulation.

It clearly shows that two modes propagate in the plate with different velocities. The faster mode is S_0 mode and the other is A_0 mode. The distance of the two modes is 190 mm approximately. According to the dispersion curve corresponding to the center frequency, the group velocities of S_0 and A_0 modes are 5291 and 3012 m⁄s, respectively. After propagating 84 μs, the theoretical distance is 191.4 mm, which is in agreement with the simulation.

The received signal is shown in Fig. 9(a). The second wavepackets owns a long time duration, which might be generated by mode superposition. Then, the mode ecomposition algorithm based on the ACPT is implemented first. The reconstructed signal from the basis functions and the error are presented in Fig. 9(a) and (b). It can be seen that the error between the reconstructed signal and the original signal is rather small. To measure the error of signal reconstruction, the quantitative results can be calculated by the following equation:

$$\mathrm{Re} = \frac{\|S_r - S_g\|_2}{\|S_g\|_2} \tag{20}$$

where Re is the error of reconstruction, S_g is the original signal, and S_r is the reconstructed signal. The error, in this case, is 0.1631. This indicates that the basis functions represent the Lamb wave signal properly.

The time–frequency is shown in Fig. 10 to present the mode decomposition more explicitly. In the second wavepacket, the direct A_0 mode and reflected S_0 mode from the plate boundary are mixed in time domain. However, they own distinct time–

frequency characteristic and they are separated by the ACPT. Therefore, the method could be effective to process modes overlapping because of boundary reflection.

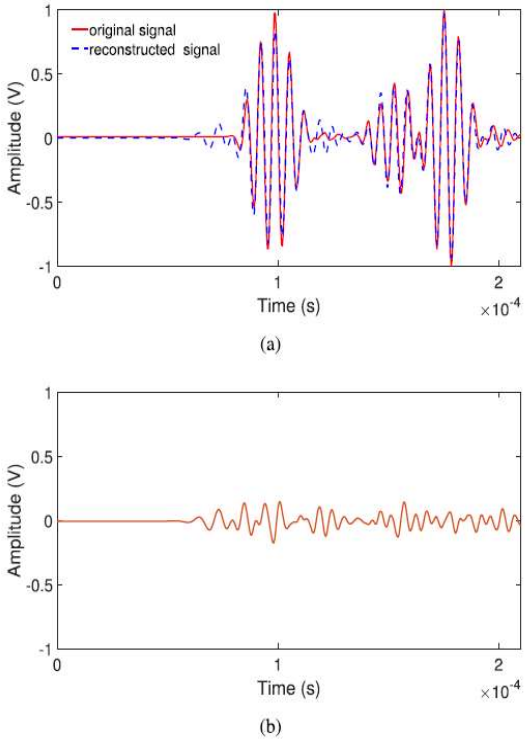

Fig. 9. Application of ACPT in the case of boundary reflection. The adaptive polynomial chirplet represents the signal properly. (a) Original signal and reconstructed signal. (b) Error between the reconstructed signal and original signal.

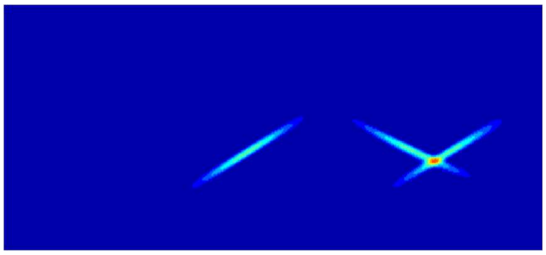

Fig. 10. Time-frequency representation of decomposed modes. The overlapped signal is separated by the ACPT.

2) Case II: The Defect With Varied Positions: The longer propagation distances of Lamb wave are investigated in this case to demonstrate the advantage of the proposed method. The only A mode is generated in the plate and the defect is also set in the right of the excitation point. The irregular shape of the defect is depicted in the finite-element model to simulate the corrosion in plate. The illustration of the model is presented in Fig. 11. The receiver point is 500 mm away from the excitation point. The defect is placed in a long distance away from the excitation point to emphasize the dispersive characteristic. The boundaries are set as the low-reflecting boundaries, and the waveform reflected from the defect is studied.

The defect in 2500 mm away from the excitation point is first simulated. The received waveform from the receiver point is shown in Fig. 12. It can be seen that three distinct wavepackets appear in the waveform. The first wavepacket denoted as P_1 is the direct wave and the other two are the reflection waves from the defect. The third wavepacket denoted as P_3 owns a larger time duration because of the dispersion.

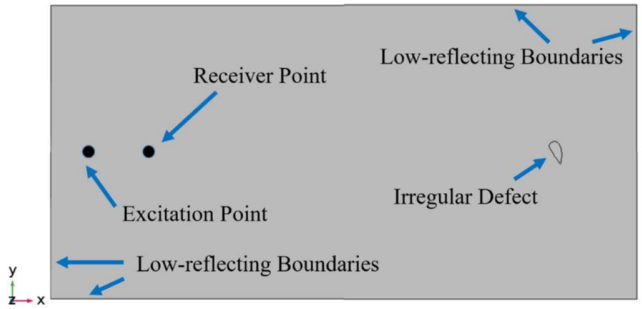

Fig. 11. Irregular defect is set in the model and the position of this defect is varied to verify the proposed method.

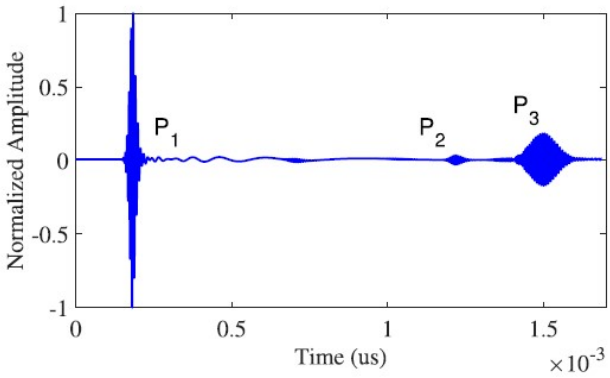

Fig. 12. Obtained waveform from the receiver point. Three distinct wavepackets can be found.

The proposed ACPT method is applied to the signal, and three basis functions are obtained. According to the information in the designed basis functions, the wavepackets of P_1 and P_3 belong to the A mode, whereas the wavepacket of P_2 belongs to the S mode. The S mode is generated from the mode conversion after the interaction of A mode with the defect. Combining the calculated amplitude, the representations of the individual modes are shown in Fig. 13(a). The two modes present different time–frequency characteristics. Furthermore, the IF curves are also shown in Fig. 13(b). It can be observed that the nonlinear relation between time and frequency is clear for the wavepacket of P_3. Through utilizing the IF curves, the TOFs corresponding to the center frequency are obtained. The TOFs of the direct A mode and reflected A mode are 182.0 and 1516.9 μs, respectively. Then, the TOF between the direct and reflected waves is 1334.9 μs. The relative error can be obtained through employing the following equation:

$$e = \frac{|\mathrm{TOF_{cal}} - \mathrm{TOF_{th}}|}{\mathrm{TOF_{th}}} \tag{21}$$

where $\mathrm{TOF_{cal}}$ is the obtained TOF from the IF curve and $\mathrm{TOF_{th}}$ is the theoretical value. According to the wave velocity, the theoretical TOF is 1327.9 μs, and then, the relative error is 0.53%.

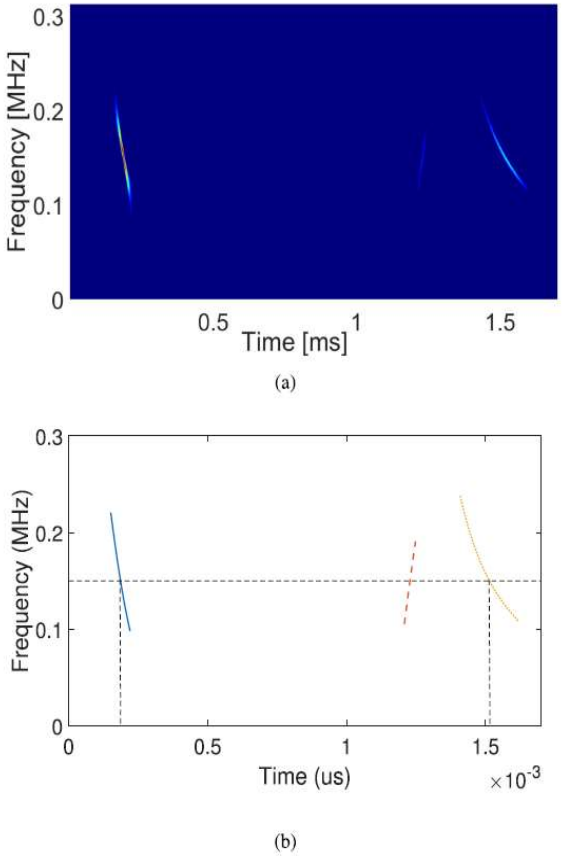

Fig. 13. Proposed method is implemented on the signal. (a) Three individual modes are depicted in the time-frequency representation. (b) Curve of IF is calculated according to the basis functions.

For comparison, the method of CT is implemented. The CT only owns the linear relation between the time and the frequency. The obtained IF curves are presented in Fig. 14. Similarly, the calculated TOFs of the direct A mode and reflected A mode are 183.2 and 1526.3μs, respectively. Then, the TOF between these two wavepackets is 1343.1μs and the relative error is 1.14%. Besides, the TOF can also be calculated from the CC of the excitation signal and the received wavepacket. The CC of the wavepacket P_3 and the excitation signal is shown in Fig. 15. The location of the maximum value in the CC indicates the time delay which is TOF for the wavepacket. Thus, the TOF of reflected A mode is 1463.6 μs. The TOF of the direct wave can be also obtained and it is 162.1 μs. Then, the TOF between wavepacket of P_1 and P_3 is 1301.5μs. The relative error is 1.99%.

The position of the defect is also varied but still in the same line with the excitation point and receiver point. The defect position is set from 1000 to 4000 mm with an increment of 500 mm. These three methods are applied to the received signal to obtain the relative error of TOF between the direct A mode and reflected A mode. The results are presented in Fig. 16. It can be seen that the error of the ACPT method is the smallest. With the increase of the defect location, the proposed method is still robust. It is also observed that when the defect location is larger than 2500 mm, which means that the propagation distance is larger than 4500 mm, the gaps of relative errors from the three methods become wider. The proposed ACPT method can adapt to the dispersive signal from longer defect location and present low error. Therefore, under the longer propagation distance where the effect brought by dispersion becomes more distinct, the proposed method owns the advantage over the other two methods.

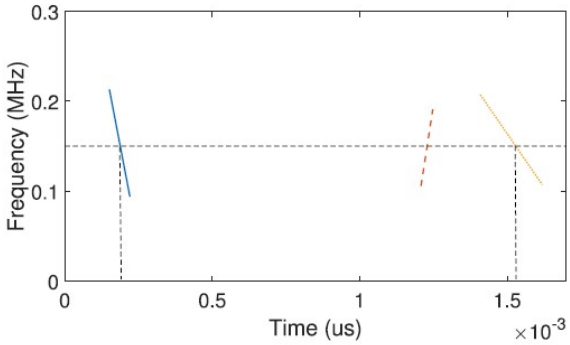

Fig. 14. Obtained IF curves from the CT. The relation between the time and frequency is linear.

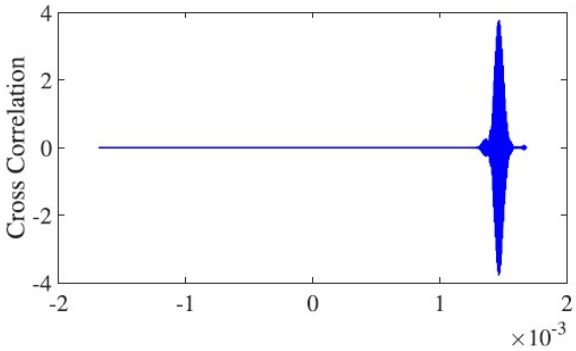

Fig. 15 CC of the wavepacket P_3 and the excitation signal.

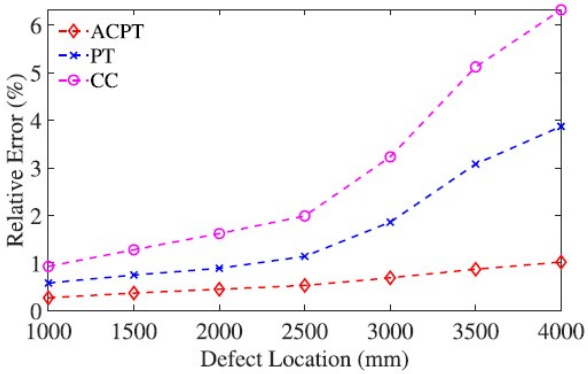

Fig. 16. Relative error of TOF between the direct A mode and reflected A mode by the application of the three methods.

B. Experiment

To consider the actual Lamb wave detection, the experiment system is established on the steel plate. The schematics are shown in Fig. 17. The RITEC RPR-4000 is adopted as the power amplifier. The EMAT is applied as the Lamb wave transmitter and receiver. They are placed in the middle part of the plate. The compositions of the EMAT are the permanent

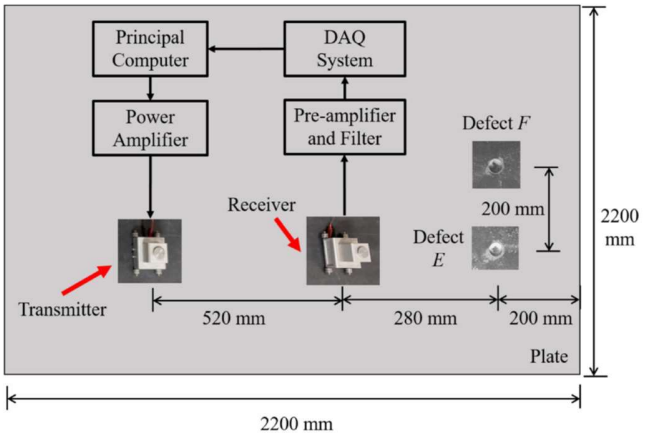

Fig. 17. Schematics of Lamb wave experiment system. The electromagnetic ultrasonic transducer is adopted as transmitter and receiver.

magnets and planar spiral coil. The received signal is first amplified and filtered by the designed signal conditioning circuits. The two-stage amplifier is used to magnify the signal by 2000 times. The fourth-order bandpass filter has the bandwidth of 20 kHz with the central frequency of 150 kHz. Then, the signal is sampled by data acquisition (DAQ) system and the sampling rate is set as 2 MHz. The same experiment is repeated by 20 times, and the received signals are averaged to rule out the noise from the environment. Finally, the data are sent to the principal computer for postprocessing. The proposed algorithm is coded in MATLAB software to process the signal. It is worth noting that the received signal from the EMAT is weak and the repetitions of the experiment contribute to increase the signal strength. The lift-off distance of the EMAT away from the plate should be low to improve the transducer response.

Two hemispherical defects machined on the plate are used to simulate the flaw of corrosion. The defect *E* lies on the straight line with the transmitter and receiver, whereas defect *F* is on the upper side of defect *E* with a distance of 20 mm. The reflection from the right boundary is studied in this case. The initial pulse signal induced by the high-power excitation signal is neglected in the following.

Because of the existences of two defects and the plate boundaries, the latter part of the signal is mixed by multiple reflections and the information value is difficult to utilize. Therefore, the former part of the signal is investigated. The received signal and reconstructed waveform are shown in Fig. 18(a). It is observed that the original signal is represented by the polynomial chirplet basis functions. From Fig. 18(b), the error of reconstruction is rather small. The calculated reconstruction error is 0.2875 by applying (20). Seven main basis functions in the dictionary are obtained using ACPT. The parameters of the basis functions are listed in Table II. The first wavepacket W_1 is represented by only one main basis function constructed from the *S* mode. The second wavepacket W_2 is decomposed into three main basis functions that are constructed from *A*, *S*, and *S* modes, respectively. The third wavepacket W_3 is represented by one main basis function from *S* mode which is boundary reflection. The fourth wavepacket W_4 is superposed by two *S* modes from the two defects.

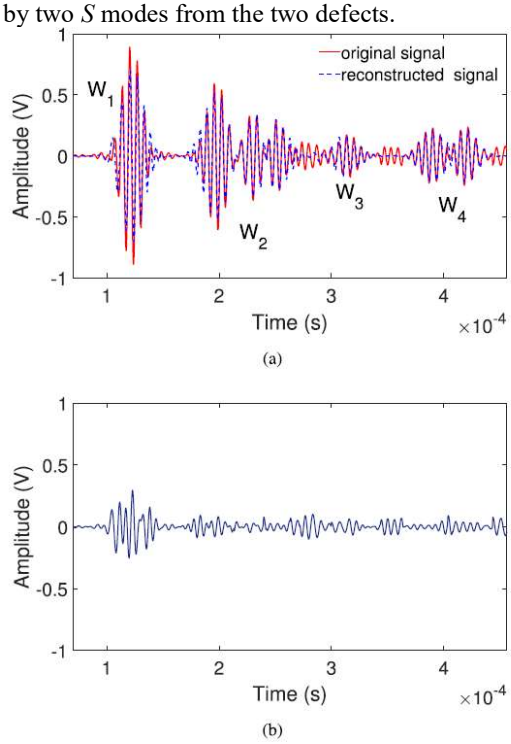

Fig.18. Application of ACPT in the case of damage reflection. The error of reconstruction is rather small. (a) Original signal and reconstructed signal. (b) Error between the reconstructed signal and original signal.

TABLE II
MAIN BASIS FUNCTIONS CONSTRUCTING THE SIGNAL

Basis Functions	Absolute Value of Amplitude (α_n)	Identified Mode
BF_1	0.33	Direct S
BF_2	0.22	Direct A
BF_3	0.11	Reflected S from defect E
BF_4	0.13	Reflected S from defect F
BF_5	0.05	Reflected S from boundary
BF_6	0.09	Reflected A from defect E
BF_7	0.08	Reflected A from defect F

The basis functions are multiplied by the calculated amplitude α_n to obtain the individual modes and they are denoted as IM_n. The visualization of the separated modes is shown in Fig. 19. The mode decomposition process clearly presents the components of the overlapped signal.

Then, the damage localization is readily accomplished by analyzing the separated mode. The IF curves of the decomposed modes are obtained by utilizing the frequency information of basis functions. The TOFs from the direct wave and reflected wave will be utilized to localize the damage. The results are shown in Fig. 20. The propagation time corresponding to te

center frequency is extracted from the IF curve. The defect E is studied first. For the S_0 mode, the times the times for direct

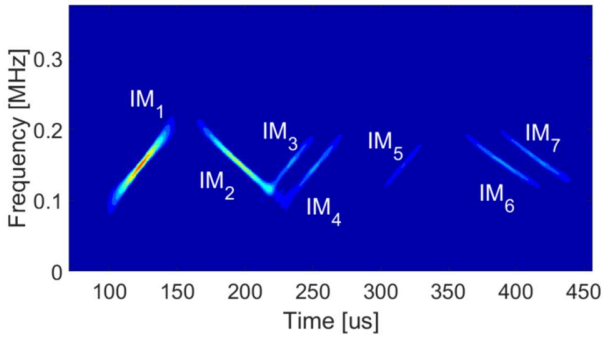

Fig. 19. Time-frequency representation of separated individual modes. The overlapped signal is decomposed and identified by the ACPT.

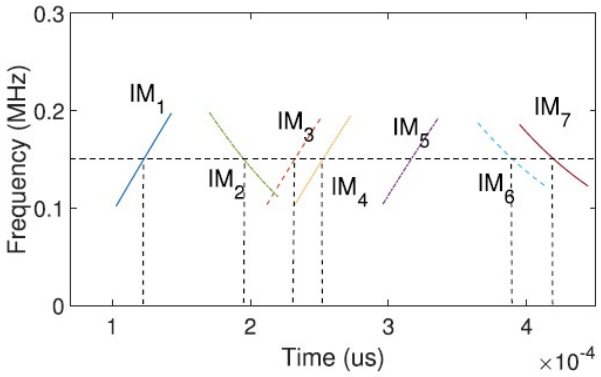

Fig. 20. Curve of IF of the individual modes.

wave and reflected wave are 122.9 and 231.4 μs, respectively. For the A_0 mode, the times are 193.5 and 385.1 μs, respectively. Then, the TOFs from the receiver to the damage are 108.5 and 191.6 μs for S_0 and A_0 modes, respectively. According to the group velocity, the location of damage from the receiver is calculated and the results are shown as follows:

$$S_0 \text{ mode}: \ d_E = 287.0 \text{ mm} \tag{22}$$

$$A_0 \text{ mode}: \ d_E = 288.5 \text{ mm} \tag{23}$$

where d_E is the calculated distance for defect E. The actual distant is 280.0 mm. The relative error can be obtained by employing the following equation:

$$e = \frac{|d_{\text{cal}} - d_{\text{th}}|}{d_{\text{th}}} \tag{24}$$

where d_{cal} is the estimated distance from the IF curve and d_{th} is the actual distance. The relative errors are 2. 51% and 3. 04% for S_0 and A_0 modes, respectively. Although there is a gap between the relative errors of the two modes, the errors are rather small and the results meet the demands of actual inspection.

In terms of defect F, the total propagation distance of the reflection wave is studied since defect F is not in the same line with the transducers. The TOFs from S_0 and A_0 modes are 29.4 and 397.2 μs, respectively. Thus, the calculated distances are 1213.8 and 1196.5 mm. The actual propagation distance from

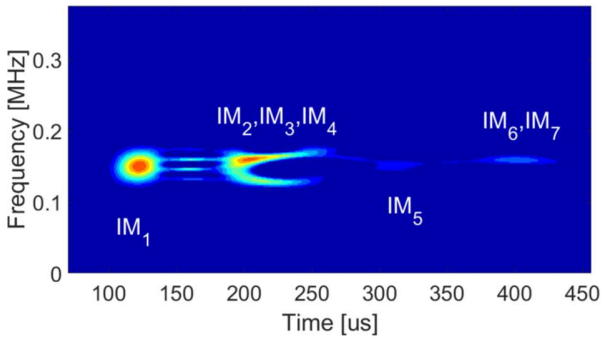

Fig. 21. Time-frequency representation of the received signal by smoothed-pseudo-WVD.

the transmitter to the damage and then reflected to receiver is 1168.7 mm. Furthermore, the relative errors are 3. 86% and 2. 38% for S_0 and A_0 modes, respectively. Although the length of the propagation route is calculated with high accuracy, this single distance is not enough to judge the position in the 2-D plate. Therefore, more receivers or the movement of the receiver are required to obtain more distance information to accomplish the localization. The least number of receivers can be determined by the corresponding mathematical model. The structure composed of multiple transmitters and multiple receivers can be adopted to further image the plate.

C. Comparison

For comparison, the WVD is applied first to demonstrate the advantage of the ACPT. WVD presents better time–frequency concentration when processing monocomponent linear frequency modulation signal. However, it brings cross terms when facing multicomponent signal, for example, the multimodal Lamb wave signals. The smoothed-pseudo- WVD is a modified version of WVD to weaken the cross terms [33]. The results for the Lamb wave in the aforementioned experiment are shown in Fig. 21. It is observed that the overlapped modes in the wavepackets influence each other and the time–frequency representation is blurred. Therefore, it is rather difficult to separate the overlapped signal by the time–frequency method.

The method of CT is also employed in the signal obtained from the experiment. The signal and reconstructed signal from the CT are presented in Fig. 22. It is clear that the error is larger than that in the ACPT. The error of the reconstruction signal is 0.3540. Similar to the localization principle, the TOF is extracted and damage location is calculated. The obtained distances are 292.4 and 295.1 mm estimated from S_0 and A_0, respectively. Then, the relative errors are 4. 43% and 5. 39%. These larger relative errors imply that the ACPT has superior performance in signal representation and damage localization. If the wave propagates a longer distance, then the signal dilation in time domain brought by the dispersion will become more severe. Thus, the nonlinear time–frequency relation will

become more distinct. The CT using the linear time–frequency chirplet will lead to larger error.

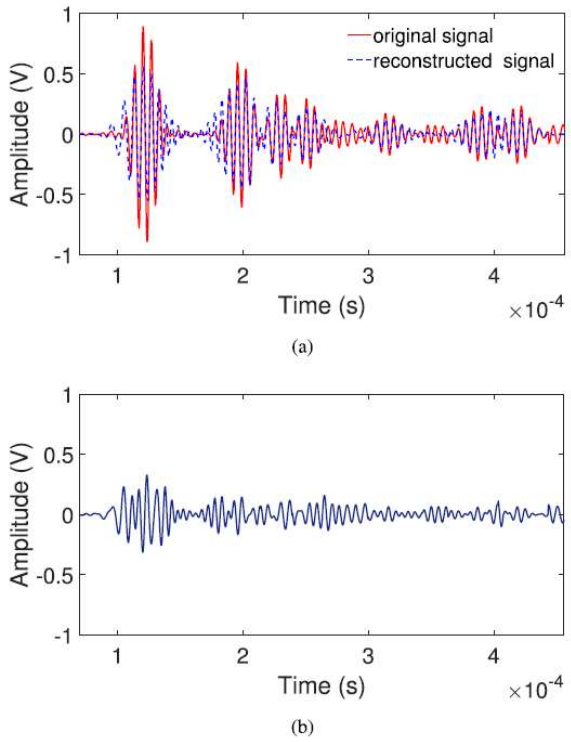

Fig. 22. Application of CT to the received signal. The error is larger than that in the proposed method. (a) Original signal and reconstructed signal. (b) Error between the reconstructed signal and original signal.

VI. CONCLUSION AND FUTURE DIRECTIONS

In this article, a new scheme of multimodal separation and identification is presented for accurate damage localization from narrowband Lamb wave. The separation of overlapped Lamb wave signals is accomplished based on the proposed ACPT method. The TOFs for the direct wave and reflected wave from damage are obtained from the IF curves.

The simulation validates that the Lamb wave signal can be effectively represented by adaptive polynomial chirplet basis functions. The error of reconstruction signal is 0.1631. Under the varied defect locations, the estimated TOFs from ACPT outperform the method of PT and CC. The proposed method is robust and the advantage is evident when the dispersive wave propagates long distances. Considering a complicated scenario in the experiment, the reconstruction error is 0.2875 in this case. For the collinear defect, the relative errors of localization are 2.51% and 3.04% estimated from S_0 and A_0 modes, respectively. For the other defect that is not in the same line with the transducers, the total propagation distance is calculated. However, the localization in the 2-D plate requires more distance information. After comparison, the reconstruction error and localization error from the CT are larger than those in the proposed ACPT. In the future work, the structure composed of multiple transmitters and multiple receivers will be studied to localize the defect in the plate. Besides, the tomography of plate structure will be implemented utilizing the decomposed modes and accurate TOFs.

REFERENCES

[1] J. Bingham and M. Hinders, "Lamb wave characterization of corrosion-thinning in aircraft stringers: Experiment and tree-dimensional simulation," *J. Acoust. Soc. Amer.*, vol. 126, no.1, pp. 103-113, Jul.2009.

[2] K.R. Leonard and M K. Hinders, "Lamb wave tomography of pipe-like structures," *Ultrasonics*, vol.43, no.7, pp.574-583, Jun. 2005.

[3] J. L. Rose, "Guided wave nuances for ultrasonic nondestructive evaluation," *IEEE Trans. Ultrason., Ferroelectr. Freq. Control*, vol. 47, no.3, pp. 575-583, May 2000.

[4] G. J.. Jarmer, E. B. Flynn, and M. D. Todd, "Multi-wave-mode, multi-frequency detectors for guided wave interrogation of plate structures," *Struct. Health Monit., Int. J.,* Vol. 13, no.2, pp.120-130, Mar. 2014.

[5] M. Mitra and S. Gopalakrishnan, "Guided wave based structural health monitoring: A review," *Smart Mater. Struct*., vol. 25, no.5, May 2016, Art, no. 05001.

[6] B. Masserey and P. Fromme, "Analysis of high frequency guided wave scattering at a fastener hole with a view to fatigue crack detection, " *Ultrasonics*, vol. 76, pp.78-86, Apr.2017.

[7] J.L. Rose, *Ultrasonic Guided Waves in Solid Media*, Cambridge, U.K.:Cambridge Univ Press, 2014.

[8] S. Wang, S, Huang, and W. Zhao, "Simulation of Lamb wave's interactions with transverse internal defects in anelastic plate, "*Ultrasonics*, vol. 51, no. 4, pp. 432-440, May 2011.

[9] S. Legendre, D. Massicotte, J. Goyette, and T. K. Bose, "Neural classification of Lamb wave ultrasonic weld testing signals using wacelet coefficients," *IEEE Trans. Instrum*. Meas., vol. 50, no.3, pp.672-678, Jun, 2001.

[10] D. Grimaldi, "Time-of-flight measurement of ultrasonic pulse echoes using wavelet networks," *IEEE Trans Instrum. Meas*., vol.55, no. 1, pp.5-13, Feb, 2006.

[11] J. -R. Lee, S. Yenn Chong, H. Jeong, and C. –W, Kong, "A time-of-flight mapping method for laser ultrasound guided in a pipe and its application to wall thining visualization," NDT E Int., vol. 44, no. 8, pp.680-691, Dec. 2011.

[12] L. Svilainis, K. Lukoseviciute, and D. Liaukonis, "Reiterative deconvolution: New technique for time of flight estimation errors reduction in case of close proximity of two reflections,"Ultrasonics, vol. 76, pp.154-165, Apr. 2017.

[13] D. Dai and Q. He, "Structure damage localization with ultrasonic guided waves based on a time-frequency method," Signal Process., vol. 96, pp.21-28, Mar. 2014.

[14] S.Legendre, D. Massicotte, J. Goyette, and T. K. Bose, "Wavelet-transform-based method of analysis for Lamb-wave ultrasonic NDE signals," IEEE Trans. Instrum. Meas., vol. 49, no.3, pp.524-530, Jun. 2000.

[15] H. Z. Hosseinabadi, B. Nazari, R. Amirfattahi, H. R. Mirdamadi, and A. R. Sadri, "Wavelet network approach for structural damage identification using guided

ultrasonic waves," IEEE Trans. Instrum. Meas., vol. 63, no. 7, pp.1680-1692, Jul. 2014.

[16] C.-B. Xu, Z.-B. Yang, X.-F. Chen, S.-H. Tian, and Y. Cie, "A guided wave dispersion compensation method based on compressed sensing," *Mech. Syst. Signal Process*., vol. 103, pp.89-104, Mar. 2018.

[17] Z. Wang, S. Huang, H. Sun, S. Wang, Q. Wang, and W. Zhao, "Multimodal Lamb wave identification using combination of instantabeous frequency with EMD, " in *Proc IEEE Int. Instrum. Meas. Technol. Conf.* (12MTC), May 2019, pp. 1-5.

[18] P. Wilcox, M. Lowe, and P. Cawley, "The effect of dispersion o long-range inspection using ultrasonic guided wave," *NDT E Int.,* vol. 34, no. 1, pp-1-9, Jan. 2001.

[19] P. D. Wilcox, "A rapid signal processing technique to remove the effect of dispersion from guided wave signals, " *IEEE Trans. Ultrason., Ferroelectr., Freq. Control*, vol. 50, no. 4, pp.419-427, Apr. 2003.

[20] W. Wu and Y. Wang, " A simplified dispersion compensation algorithm for the interpretation of guided wave signals, " *J. Pressure Vessel Tech- nol.,* vol. 141, no.2, Apr, 2019, Art. No.021204.

[21] P. D. Wilcox, M. J. S. Lowe and P. Cawley, "Mode and transducer selection for long range Lamb wave inspection," *J. Intell. Mater. Syst. Struct.,* vol. 12, no. 8, pp. 553-565, Aug.2001.

[22] J. L. Rose, S. P. Pelts, and M. J. Quarry, "A comb transducer model for guided wave NDE, "*Ultrasonics*, vol. 36, nos. 1-5, pp.163-169, Deb. 1998.

[23] R.S.C. Monkhouse, P. D. Wilcox, and P. Cawley, "Flexible interdigital PVDF transducers for the generation of Lamb waves in structures, "*Ultrasounics*, vol. 35, no.7, pp. 489-498, Nov. 1997.

[24] Z. Liu, Y. Hu, M. Xie, B. Wu, and C. He, "Development of omnidirectional a 0 mode EMAT employing a concentric permanent magnetpairs with opposite polarity for plate inspection," *NDT E Int*., vol.94, pp.13-21, Mar.2018.

[25] A. Raghavan and C.E.S. Cesnik, "Guided-wave signal processing using chirplet matching pursuits and mode correlation for structural health monitoring," *Smart Mater. Struct.,* vol. 16, no.2, pp.355-366, Apr. 2007.

[26] A. B. Zoubi, S. Kim, D. O. Adams, and V, J. Mathews, "Lamb wave mode decomposition based on cross-Wigner-Ville distribution and its application to anomaly imaging for structural health monitoring," *IEEE Trans Ultrason., Ferroelectr., Freq. Control,* vol. 66, no.5, pp.984-997, May 2019.

[27] M.Zhao, L. Zeng, J. Lin, and W. Wu, "Mode identification and extraction of broadband ultrasonic guided waves," *Meas. Sci. Technol.,* vol.25, no.11, Nov. 2014, Art, no. 115005.

[28] L. Zeng, M.Zhao J. Lin, and W. Wu, "Waveform separation and image fusion for Lamb waves inspection resolution improvement, "*NDT E Int*., vol.79, pp.17-29, Apr. 2016.

[29] Y. Zhang, S. Huang, S. Wang, Z. Wei, and W.Zhao, "Recognition of overlapped Lamb wave detecting signals in aluminum plate by EMD-based STFT flight time extraction method." *Int. J. Appl. Electromagn. Mech*., vol. 52. Nos. 3-4, pp.991-998, Dec. 2016.

[30] D. N. Alleyne and P. Cawley, "The interaction of Lamb waves with defects," IEEE Trans. Ultrason., Ferroelectr., Freq. Control, vol.39, no. 3, pp.381-397, May 1992.

[31] Y. Cho, D. D. Hongerholt, and J. L. Rose, "Lamb wave scattering analysis for reflector characterization," IEEE Trans. Ultrason., Ferroelectr., Freq. Control, vol.44, no. 1, pp.44-52, Jan. 1997.

[32] J. Ville, "Theorie et application data notion de signal analytique," Câbles Transmiss., vol. 2, no.1, pp.61-74, 1948.

[33] F. Auger and P. Flandrin, "Improving the readability of time-frequency and time-scale representations by the reassignment method," IEEE Trans. Signal Process., vol. 43, no.5, pp.1068-1089, May 1995.